Contents

1 Extensive air showers

Extensive air showers describe the particle cascades that are the result of a high-energy cosmic ray interacting with the atmosphere of the earth. While the microstate of a given air shower is inherently chaotic, macroscopic variables such as the number of particles in the cascade, its' multiplicity, allow conclusions on the primary cosmic ray.

In this chapter the various processes which give raise to the jets of energetic particles are discussed. Because hadronic primaries that carry intrinsic SU(3)-color charges are fundamentally different from leptonic ones which do not, this is done in a two-fold way. The funamental principles giving rise to electromagnetic cascades are shown in section 1.1. Supplementary information regarding hadronic showers is listed in section 1.2. Finally, the effect of differing hadronic primaries is considered in section 1.3.

1.1 Electromagnetic showers

The dominating interaction of $E > 10\,\mathrm{MeV}$ photons in matter is e^+e^- pair production, whereas for electrons/positrons the creation of a γ via bremsstrahlung prevails at high energies. This is shown in Figure 1.1. Consequently, an entire cascade of $e^\pm$ and photons can emerge from a single primary particle, as realised by Heitler in [3].

Of particular interest in these showers are, apart from the primary particles energy E_0 and arrival direction (Φ, θ), the atmospheric depth X_max at which it reaches its' maximum multiplicity, as well as the **L**ateral **D**istribution **F**unction (LDF), that parametrizes the distribution of particles along the shower axis. An important variable that influences both values is the radiation length X_0. It represents the characteristic length at which an $e^\pm$ loses $1 - \frac{1}{e} \approx 63\%$ of its energy. It also corresponds to the mean free path of a photon in matter up to a factor 7/9 [**gupta2010calculation**]. Neglecting said factor and assuming that new particles on average inherit half of the parent energy, describing the multitude of particles contained in an electromagnetic shower becomes a counting exercise in the context of the Heitler-model.

With each radiation length, the number of particles N in the shower double, while the energy per particle E_pp halves. After traversing an atmospheric depth of $n \cdot X_\mathrm{max}$, typically measured in units of $\frac{\mathrm{g}}{\mathrm{cm}^2}$, they consequently read

$$N(n) = 2^n, \qquad E(n) = \frac{E_0}{2^n}. \tag{1.1}$$

After sufficient interactions, the energy of each individual particle E_PP will have degraded to such an extent that other processes are no longer negligible compared to

(a) γ interactions

(b) $e^{\pm}$ interactions
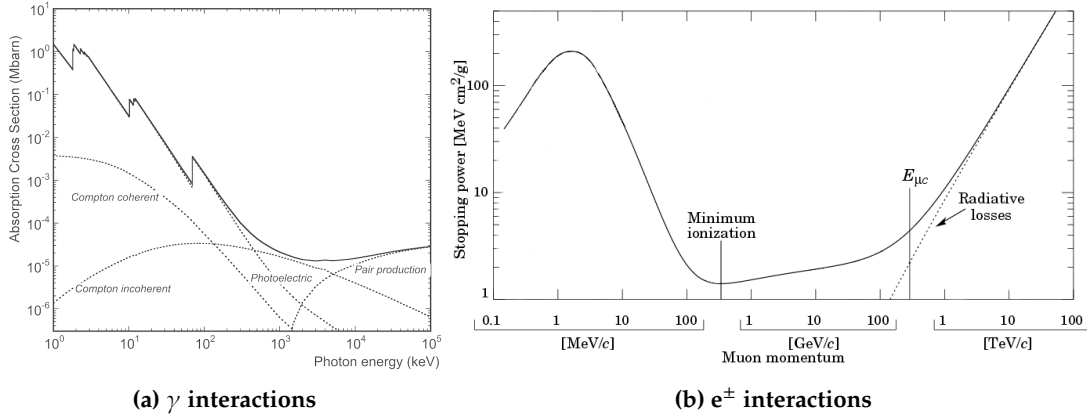
Figure 1.1: (a) Cross section for different energy loss processes of a photon in tungsten. The sudden spikes correspond to the transition energy of increasingly higher-energy electron shells. From [1]. **(b)** Stopping power of copper, representatively on an antimuon μ^+, with respect to its' momentum. Plot adopted with changes from [2].

bremsstrahlung and pair production. This occurs at the critical energy $E_{c,\text{EM}}$ below which the shower rapidly stops creating new particles and dies out as a result. It follows via Equation 1.2 and 1.3 that both $X_{\max}$ as well as $N_{\max}$ increase with E_0. The multiplicity arising from these assumptions alongside a stylized propagation of the thus created shower is represented in Figure 1.2.

$$E_{\text{PP}}\left(n_{\max}\right) \overset{!}{=} E_c \overset{(1.1)}{=} \frac{E_0}{2^{n_{\max}}}$$

$$\Leftrightarrow \qquad n_{\max} = \left\lfloor \log_2\left(\frac{E_0}{E_{c,\text{EM}}}\right) \right\rfloor$$

$$\Rightarrow \qquad X_{\max} = n_{\max} \cdot X_0 = \left\lfloor \log_2\left(\frac{E_0}{E_{c,\text{EM}}}\right) \right\rfloor . \tag{1.2}$$

$$\Rightarrow \qquad N_{\max} = 2^{n_{\max}} = \left\lfloor \frac{E_0}{E_{c,\text{EM}}} \right\rfloor . \tag{1.3}$$

The number of particles at a given distance from the shower axis (y-axis in Figure 1.2) is essentially random, but follows a statistical basis, the lateral distribution function. The LDF can either be derived approximately from first principles [4] or empirically, as is done in [5]. The latter arrives at a closed form approximation for the local density ρ of particles given a shower with multiplicity N at a distance r from the shower axis as

$$\rho_{\text{EM}}(N, r) = \frac{0.4\,N}{r_{\text{M}}^2}\left(\frac{r_{\text{M}}}{r}\right)^{0.75}\left(\frac{r_{\text{M}}}{r + r_{\text{M}}}\right)^{3.25}\left(1 + \frac{r}{11.4\,r_{\text{M}}}\right) . \tag{1.4}$$

In Equation 1.4, the Molière radius r_{M} characterizes the lateral spread in multiple scattering processes. It is of order $r_{\text{M}} \approx 100\,\text{m}$ for interactions that are relevant here, and in general depends on the density of the considered material [6].
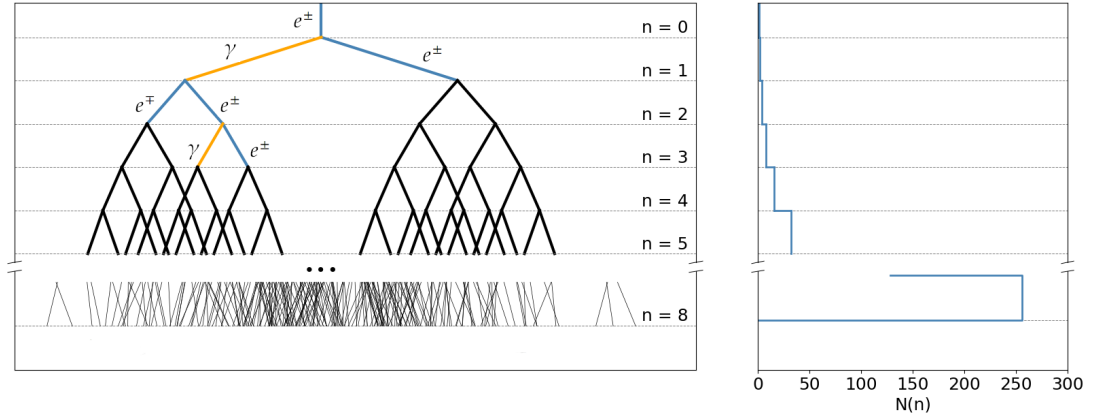
Figure 1.2: Shown on the left is the stylized propagation of an extensive air shower through the atmosphere according to the Heitler-model, quantized in units of X_0. The energy of the primary particle is of order $2^8 \cdot E_{c,\,EM}$, which allows for 8 bifurcation steps, and N_{max} = 256 shower particles. The multiplicity of the shower after each step is shown in the right subplot.

1.2 Hadronic showers

Hadronic primaries will readly produce color-charged secondaries, as has been shown many times in particle accelerators. In order to model the development of hadronic showers, the model discussed in Equation 1.1 thus needs to be adjusted. An example theory has been developed by Matthews in 2005. Following the reasoning in [7], after traversing an atmospheric depth corresponding to the hadronic interaction length, a proton creates on average $N_\pi \approx 15$ pions, of which two thirds are charged, and one third is uncharged. The corresponding decay channels of the light π-mesons with the largest **B**ranching **R**atios (BR) are

$$\pi^+ \rightarrow \mu^+ + \nu_\mu \qquad (\text{BR} \approx 0.9999,\ \tau = 2.6033 \times 10^{-8}\,\text{s [8]}),$$
$$\pi^- \rightarrow \mu + \bar{\nu}_\mu \qquad (\text{BR} \approx 0.9999,\ \tau = 2.6033 \times 10^{-8}\,\text{s [8]}),$$
$$\pi^0 \rightarrow 2\gamma \qquad (\text{BR} \approx 0.9882,\ \tau = 8.5 \times 10^{-17}\,\text{s [8]}).$$

With a mean lifetime of just attoseconds, the π^0 decay instantly before being able to continue the cascade process. In this fashion, the uncharged particles initiate a Heitler shower such as the one in section 1.1, by providing high-energy photons. It follows that every hadronic shower has an electromagnetic component. Moreover, assuming that the inherited energy from the parent particle is roughly uniformly distributed among its' children, one third of the remaining energy in the hadronic component is lost to the electromagnetic component per hadronic interaction length.

Meanwhile, the charged pions repeat the procedure of creating secondary mesons, kicking off the hadronic component of the shower in the process.

Similar to the reasoning in section 1.1, a primary of given energy initiates a shower of a specific multiplicity $N_{\max}$. This is reached after $n_{\max}$ steps, where the energy per particle $E_{\mathrm{PP}}(n_{\max})$ is below the critical energy $E_{c,\,\mathrm{had.}}$ at which the mesons ionize rather than continue the cascade. After this last step, the charged pions eventually decay into muons and neutrinos. The shower characteristics are thus given by

$$N_{\mathrm{had}}(n) = \left(\frac{2\,N_\pi}{3}\right)^n, \qquad E_{\mathrm{PP}}(n) = \frac{E_0}{N_\pi^n}, \qquad n_{\max} = \left\lfloor \log_N\left(\frac{E_0}{E_{c,\,\mathrm{had}}}\right) \right\rfloor, \qquad (1.5)$$

wheras the maximum multiplicity (ignoring neutrinos) in the shower is calculated as

$$N_{\max,\,1} = \underbrace{\frac{3}{2}\left(\frac{2}{3}N_\pi\right)^{n_{\max}}}_{\text{Muon component}} + \underbrace{\sum_{k=1}^{n_{\max}-1} \frac{N(k)}{3}\cdot\left\lfloor\frac{E_{\mathrm{PP}}(k)}{E_{c,\,\mathrm{EM}}}\right\rfloor}_{\text{EM component}}. \qquad (1.6)$$

The muons stemming from pion decay follow a different LDF than the electromagnetic component. Again following the analysis in [5], the muonic LDF can be recovered as

$$\rho_\mu(N,t) = 18\left(\frac{N}{10^6\cdot r}\right)^{\frac{3}{4}}\cdot\left(1+\frac{r}{320}\right)^{-\frac{5}{2}}. \qquad (1.7)$$

While the above Equation 1.7 drops off slower $O(r^{-\frac{3}{2}})$ compared to the electromagnetic component ($O(r^{-3})$), the immediate vicinity of the shower axis contains mostly photons and leptons from the EM subshower. Further out, the muonic component takes over. This is visualized in Figure 1.3. Due to this reason, and the fact that muons can carry considerable amounts of energy faraway from the shower axis, the muonic footprint of a shower often appears much more "patchy" compared to the EM portion. This knowledge is espically useful when distinguishing between hadron- and photon-induced air showers (compare [9]).

Where did the better picture go??

1.3 Composite primaries

As is evident from the discussion in **??**, not only single protons (which are strictly speaking also composite) or elementary particles like photons, electrons, etc. appear in the cosmic ray spectrum. In theory, any somewhat stable particle is a possible primary. The consequence of different primaries on resulting shower characteristics is subtle, but large enough such that it can be used for identification purposes.

Assuming the constituents in a CR nucleus all coherently interact with an air molecule, one arrives at the superposition principle for extensive air showers. It states that for a composite primary with $A = N + Z$ neutrons and protons, each constituent particle
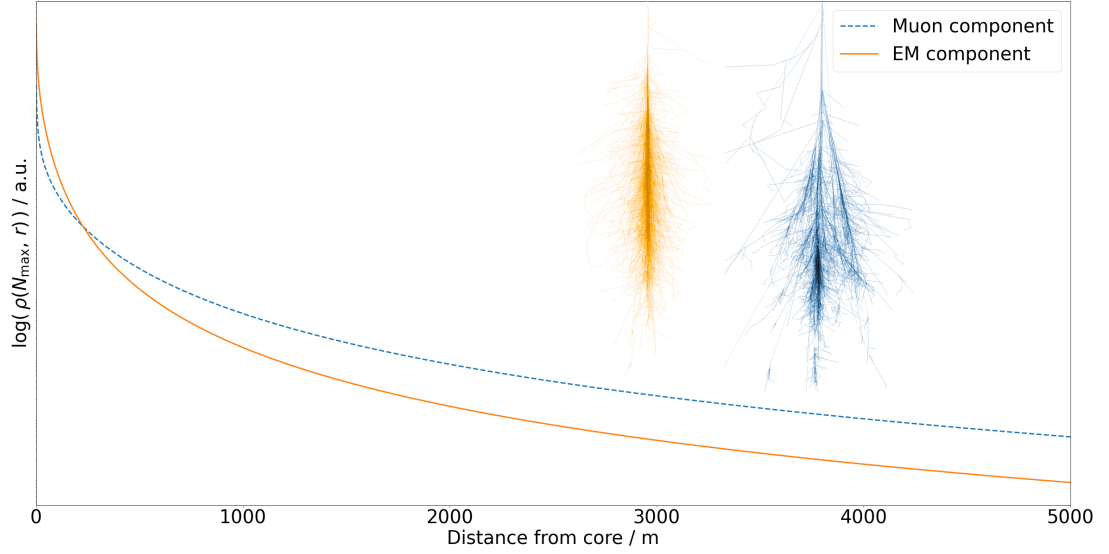
Figure 1.3: The lateral distribution function for the muonic (steelblue) and electromagnetic (orange) component of a vertical, 100 GeV proton shower at roughly sea level ($r_M = 100\,\text{m}$). The inset plots on the top-right represent the xz-projection of the shower shape. Both images adopted with changes from [10].

will initiate a shower with initial energy of $E_0' = E_0 \,/\, A$, where E_0 is the initial energy of the composite particle. For this scenario, N_{max} and n_{max} are known from the preceding sections. It follows that air showers from heaver primaries occur at higher altitudes (lower atmospheric depth X) and with higher particle counts.

$$N_{\text{max}, A} = A \cdot N_{\text{max}}, \qquad n_{\text{max}, A} = \left\lfloor \log_N \left(\frac{E_0}{E_{c, \text{had}}} \right) - \log_N A \right\rfloor, \tag{1.8}$$

where $N_{\text{max}, A}$, $n_{\text{max}, A}$ refer to the resulting extensive air shower characteristics that are induced by a particle with mass number A.

1.4 Comments on validity

The Heitler model and Heitler-Matthews model discussed in section 1.1 and section 1.2 respectively make only very rudimentary assumptions on the underlaying physics of particle cascades. Nevertheless, the equations recovered from these assumptions are already a close approximation of real world processes up to X_{max}.

Of course, adding a stochastic component to the above assumptions (c.f. [11]) improves predictions. But even full-fledged Monte-Carlo simulation software frameworks like GEANT4 [12] or CORSIKA [13] show discrepancies between observed and predicted shower development when analysed in depth. This is shown in Figure 1.4.

While shower-to-shower fluctuations can explain discrepancies to a degree, there also exist systematic differences between the simulated and observed extensive air showers.
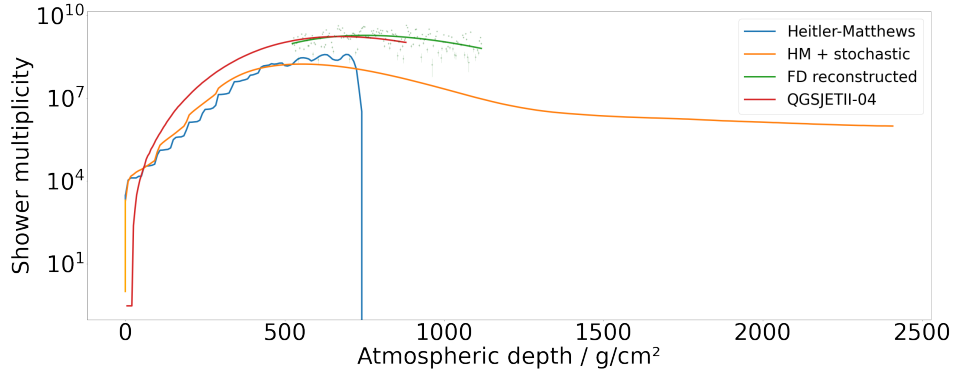
Figure 1.4: Comparison of the number of charged particles for different physics models to reconstructed observations from a 3 EeV proton shower. Shown in steelblue and orange is the Heitler-Matthews model as described in section 1.2, and extended with a stochastic component. An example of a more in-depth simulation in red, and observed shower multiplicities in green.

These are largely owed to imprecise knowledge of the underlaying physical processes. For example, hadronic interaction models (e.g. QGSJETII-04) rely on extrapolation of measured cross sections in the GeV-TeV scales to the relevant CR energies [14]. While this is not an unfair assumption given the scale invariance of deep inelastic scattering [15], it is clear, that the approach cannot accurately encompass all effects that may take place at the high energies present in atmospheric particle cascades.

In conclusion, the particle cascades evolving from relativistic CRs impinging on earth are still not fully understood. Several simulation frameworks have been developed, which each have their own shortcomings. It is therefore important to compare not only results from simulations using one framework to observations, but also different simulations with each other.

1.5 Detection methods

1.5.1 Cherenkov light

When a charged particle exceeds the phase velocity of light in a medium with refractive index n, the optical equivalent of a sonic boom occurs. Photons travel in a shockwave along an angle $\theta = \arccos\left(n^{-1}\beta^{-1}\right)$ relative to the trajectory of the particle while $\beta \geq \frac{c}{n}$. This process is well understood and can be used to detect high energy cosmic rays.

Imaging Air Cherenkov Telescope

The refractive index of air ranges from 1 in the near vacuum of the upper atmosphere to $\approx 1 + 2.9 \cdot 10^{-4}$ at sea level [16]. This implies that particles with a Lorentz factor

$\gamma \gtrsim 41.5$ emit Cherenkov light, which is satisfied for e.g. muons and protons in the low GeV ranges and above.

It can therefore be expected that extensive air showers, which contain high energy charged particles, produce considerable amounts of Cherenkov light when propagating throught the atmosphere. This light, and by extension the air shower can be detected with **I**maging **A**ir **C**herenkov **T**elescopes (IACTs). Ground based experiments such as VERITAS [17] or H.E.S.S [18] detect gamma-rays using this technique.

Water Cherenkov Detector

The lightspeed in water is roughly 33% slower than in vacuum. Cherenkov radiation in water therefore occurs more easily than in air. Using this reasoning, a water tank equipped with means of detecting the emitted Cherenkov light, via e.g. **P**hoto**M**ultiplier **T**ubes (PMTs), should be able to measure traces of an air shower.

Indeed, this exact measurement principle of a **W**ater **C**herenkov **D**etector (WCD) was and is adopted in a variety of cosmic ray observatories such as the Pierre Auger observatory [19], HAWC [20], or Kamiokande [21], for example.

1.5.2 Fluoresence

Ionization losses have been ignored in the discussion of the formation of extensive air showers. This is of course not completely accurate. During the development of an extensive air showers, particles excite, or even ionize the permeated medium. Consequently, spontaneous emission of photons due to recombination, or transition back to a ground state can be observed. The amount of fluorescence light produced in this way is a gauge for the number of particles present in the shower at a given moment.

In Air

The predominant element in air is nitrogen (78%), whose transitions lay in the UV-band [22]. After a nitrogen molecule is excited by a passing shower particle, a photon with wavelength $300\,\text{nm} \leq \lambda \leq 430\,\text{nm}$ is emitted isotropically due to relaxation. The low attenuation of ultraviolet radiation in air allows the fluorescence light to travel large distances before being absorbed [23]. This enables cameras like EUSO-TA [24] or the **F**lourescence **D**etector (FD) of the Pierre Auger observatory (see [22] and **??**) to observe traces of extensive air showers from faraway during their development.

However, because of the low light yield of just $5\,\text{photons/MeV}$ [25], the detectors must operate in low UV-noise conditions, which places an upper limit on their duty cycle.

In Scintillators

Conventional plastic scintillators have a light yield, that is $1000-10000$ times higher than that of air [26]. Such scintillators therefore pose an effective way of measuring a shower footprint on the ground. The Pierre Auger **S**urface **D**etector (SD) is equipped with scintillators during the ongoing AugerPrime upgrade. Predecessors like KASCADE [27] have been using scintillation light to detect cosmic rays as well.

1.5.3 Radio Emission

Relativistic charged particles in the cascade are subject to deflections due to the geomagnetic field. This deflection is largest for $e^\pm$ due to their comparably tiny masses. Albeit the deflection of a typical electron in the shower is miniscule and the subsequent emission of Bremsstrahlung tiny, coherence effects along the entire shower front can greatly amplify the electric field strengths obtained from this effect [28]. This gives rise to radio signals emitted by the extensive air shower, which can in principle be detected via antennas.

One challenge in constructing an efficient CR radio detector is the requirement for a radio-quiet environment, where a large enough **S**ignal-to-**N**oise-**R**atio (SNR) permits analysis of measured data. This is the case for the AERA component of the Pierre Auger observatory, which has been in operation since 2010 [29]. Its results have in part lead the proposal of a vast radio array, GRAND [30], which will have an enormous exposure to CR showers, if built.

Bibliography

[1] Sow-Hsin Chen and Michael Kotlarchyk. *Interactions of photons and neutrons with matter*. World Scientific, 2007.

[2] Stefano Meroli. "The Straggling function. Energy Loss Distribution of charged particles in silicon layers". In: *Home Cern, https://meroli. web. cern. ch/lecture_- StragglingFunction. html* (2017).

[3] Walter Heitler. *The quantum theory of radiation*. Courier Corporation, 1984.

[4] Koichi Kamata and Jun Nishimura. "The lateral and the angular structure functions of electron showers". In: *Progress of Theoretical Physics Supplement* 6 (1958), pp. 93–155.

[5] Kenneth Greisen. "Cosmic ray showers". In: *Annual review of nuclear science* 10.1 (1960), pp. 63–108.

[6] Gert Moliere. "Theorie der streuung schneller geladener teilchen i. einzelstreuung am abgeschirmten coulomb-feld". In: *Zeitschrift für Naturforschung A* 2.3 (1947), pp. 133–145.

[7] James Matthews. "A Heitler model of extensive air showers". In: *Astroparticle Physics* 22.5-6 (2005), pp. 387–397.

[8] Particle Data Group et al. "Review of Particle Physics". In: *Progress of Theoretical and Experimental Physics* 2020.8 (Aug. 2020). 083C01. ISSN: 2050-3911. DOI: 10.1093/ptep/ptaa104. eprint: https://academic.oup.com/ptep/article-pdf/2020/8/083C01/34673722/ptaa104.pdf. URL: https://doi.org/10.1093/ptep/ptaa104.

[9] Tomás Capistrán, I Torres, and L Altamirano. "New method for Gamma/Hadron separation in HAWC using neural networks". In: *arXiv preprint arXiv:1508.04370* (2015).

[10] Fabian Schmidt. *Sample Corsika showers.* https://www.zeuthen.desy.de/~jknapp/fs/proton-showers.html. Accessed: 08th Dec. 2022.

[11] Martin Pittermann and Paul Filip. *Simple hadronic shower simulation in C++.* https://github.com/martin2250/showersim. Accessed: 13th Dec. 2022.

[12] Sea Agostinelli et al. "GEANT4—a simulation toolkit". In: *Nuclear instruments and methods in physics research section A: Accelerators, Spectrometers, Detectors and Associated Equipment* 506.3 (2003), pp. 250–303.

[13] Dieter Heck et al. "CORSIKA: A Monte Carlo code to simulate extensive air showers". In: *Report fzka* 6019.11 (1998).

[14] S Ostapchenko. "QGSJET-II: towards reliable description of very high energy hadronic interactions". In: *Nuclear Physics B-Proceedings Supplements* 151.1 (2006), pp. 143–146.

[15] DJ Fox et al. "Early tests of scale invariance in high-energy muon scattering". In: *Physical Review Letters* 33.25 (1974), p. 1504.

[16] Larry C Andrews. "An analytical model for the refractive index power spectrum and its application to optical scintillations in the atmosphere". In: *Journal of Modern Optics* 39.9 (1992), pp. 1849–1853.

[17] The VERITAS Collaboration. *VERITAS Telescope Homepage*. `https://veritas.sao.arizona.edu/`. Accessed: 26th Dec. 2022.

[18] The H.E.S.S. Collaboration. *H.E.S.S. Telescope Homepage*. `https://www.mpi-hd.mpg.de/hfm/HESS/`. Accessed: 26th Dec. 2022.

[19] The Pierre Auger Collaboration. *Pierre Auger Observatory Homepage*. `https://www.auger.org/`. Accessed: 26th Dec. 2022.

[20] The HAWC Collaboration. *HAWC Observatory Homepage*. `https://www.hawc-observatory.org/`. Accessed: 26th Dec. 2022.

[21] The Kamiokande Collaboration. *Super-Kamiokande Homepage*. `https://www-sk.icrr.u-tokyo.ac.jp/en/sk/`. Accessed: 26th Dec. 2022.

[22] Jorge Abraham et al. "The fluorescence detector of the Pierre Auger Observatory". In: *Nuclear Instruments and Methods in Physics Research Section A: Accelerators, Spectrometers, Detectors and Associated Equipment* 620.2-3 (2010), pp. 227–251.

[23] Louis Elterman. *UV, visible, and IR attenuation for altitudes to 50 km, 1968*. Tech. rep. AIR FORCE CAMBRIDGE RESEARCH LABS HANSCOM AFB MA, 1968.

[24] Ghouti Abdellaoui et al. "EUSO-TA–First results from a ground-based EUSO telescope". In: *Astroparticle Physics* 102 (2018), pp. 98–111.

[25] M Nagano et al. "New measurement on photon yields from air and the application to the energy estimation of primary cosmic rays". In: *Astroparticle Physics* 22.3-4 (2004), pp. 235–248.

[26] Ina Holl, Eckart Lorenz, and Gikas Mageras. "A measurement of the light yield of common inorganic scintillators". In: *IEEE Transactions on Nuclear Science* 35.1 (1988), pp. 105–109.

[27] The KASCADE Collaboration. *KASCADE Homepage*. `https://www.iap.kit.edu/kascade/index.php`. Accessed: 26th Dec. 2022.

[28] Alexander Aab et al. "Observation of inclined EeV air showers with the radio detector of the Pierre Auger Observatory". In: *Journal of Cosmology and Astroparticle Physics* 2018.10 (2018), p. 026.

[29] The Pierre Auger Collaboration. *AERA - Auger Engineering Radio Array*. `https://auger.org/observatory/aera`. Accessed: 18th Jan. 2023.

[30] Jaime Álvarez-Muñiz et al. "The giant radio array for neutrino detection (GRAND): science and design". In: *Science China Physics, Mechanics & Astronomy* 63.1 (2020), pp. 1–43.